# Parameterized convection, grid-scale clouds and resolution sensitivity in the Community Atmosphere Model

Adam R. Herrington*, Kevin A. Reed

*School of Marine and Atmospheric Sciences, Stony Brook University, Stony Brook, NY 11794*

*Correspondence to: adam.herrington@stonybrook.edu

## This paper describes...

*Key Words:* Climate models, physical parameterizations, physics-dynamics coupling

*Received* . . .

## 1. Introduction

An increasing number of Atmospheric General Circulation Models (AGCMs) are being developed to maximize efficiency on massively parallel systems, permitting regionally-refined high-resolution, or even globally high-resolution weather ($\Delta x = 5$ km and less) and climate ($\Delta x = 50$ km and less) simulations (Skamarock *et al.* 2012; Zängl *et al.* 2014; Harris *et al.* 2016; Ullrich *et al.* 2017; Lauritzen *et al.* 2018). These models are built using unstructured meshes that while allows for substantial grid flexibility, would require physical parameterizations (*physics*) that behave consistently as the truncation scale of the model changes with different grid resolutions, referred to as scale-aware physics. The most common approach towards developing scale-aware physics is through the lens of limited area, large-eddy simulations (e.g., Plant and Craig 2008; Arakawa and Wu 2013; Song and Zhang 2018). Through subsequently filtering large-eddy solutions to lower-resolution grids, a relationship between first- and higher-order moments (Germano 1992) may be understood and ultimately parameterized as a function of grid resolution. While this approach is likely necessary for developing scale-aware physics, it is not sufficient. The equations of motions have inherent scale dependencies, with the properties of dynamical modes a function of native grid resolution (Orlanski 1981; Weisman *et al.* 1997; Pauluis and Garner 2006; Jeevanjee and Romps 2016). Scale-aware physics should also recognize these native grid dependencies.

The sensitivity of the Community Atmosphere Model (CAM; Neale *et al.* 2012), and its predecessor, the Community Climate Model (CCM) to resolution (*resolution* refers to *horizontal resolution*, hereafter) is well documented through convergence studies (Kiehl and Williamson 1991; Williamson *et al.* 1995; Williamson 2008; Rauscher *et al.* 2013; Zarzycki *et al.* 2014; Herrington and Reed 2017). Despite thirty years of continual model development, there are robust sensitivities to resolution that have persisted in all versions of the model. This study argues that a unifying cause, the inherent scale sensitivities of the underlying dynamical equations, can explain the robust responses to resolution that occur in CAM/CCM, since it is difficult to conceive that inevitable responses to native grid resolution could be ignored in the pursuit of scale-aware physics.

In CAM/CCM, the atmosphere progressively dries with increasing resolution, seen through a reduction in simulated total precipitable water (Kiehl and Williamson 1991; Williamson *et al.* 1995; Williamson 2008; Rauscher *et al.* 2013; Zarzycki *et al.* 2014; Herrington and Reed 2017), which typically, but not always (see Williamson *et al.* 1995; Zarzycki *et al.* 2014), coincides with a reduction in cloud cover. Kiehl and Williamson (1991) and Williamson *et al.* (1995) suggested that the drying of the atmosphere is due to greater magnitude resolved vertical velocities with increasing resolution, with greater subsiding motion increasing the export of dry air from the upper troposphere. This mechanism is consistent with an analysis of moisture budgets in CAM, version 4 (CAM4; Neale *et al.* 2010) across multiple resolutions (Yang *et al.* 2014; Herrington and Reed 2017).

It is well known that the magnitude of vertical velocities increase with resolution in atmospheric models. While the cause of this sensitivity has been established for large-eddy simulations (see Jeevanjee 2017, and references therein), only recently has the vertical velocity field in AGCMs and their sensitivity to resolution received attention (Donner *et al.* 2016; O'Brien *et al.* 2016), albeit with conflicting explanations (Rauscher *et al.* 2016; Herrington and Reed 2018). To generalize the relationship between vertical velocity and resolution, let $\alpha$ refer to the ratio of $W_0$, the vertical velocity scale of some reference grid spacing $\Delta x_0$, to $W$, the vertical velocity scale of any $\Delta x$. A power law for $\alpha$ in $\Delta x$ is then,

$$\alpha = \frac{W_0}{W} = \left(\frac{\Delta x_0}{\Delta x}\right)^n, \tag{1}$$

where $n$ is the power law exponent.

Rauscher *et al.* (2016) derive an estimate $n = b - 1$ by combining a scale analysis of the continuity equation with a power law representation $\Delta x^{2b}$ of the second-order structure function of the horizontal wind. Strictly speaking, $\Delta x$ here refers to the distance between two points for which the velocity increment is computed in the structure function, but with this distance set to the model grid-spacing. Observations indicate that $b = \frac{1}{3}$ for scales less than about 1000 km (Cho *et al.* 1999), which according to the Weiner–Khinchin theorem $-(2b + 1) = -\frac{5}{3}$ is equal to the slope of the kinetic energy spectrum, which is true for observations of mesoscale flow (Nastrom and Gage 1985). Rauscher *et al.* (2016)

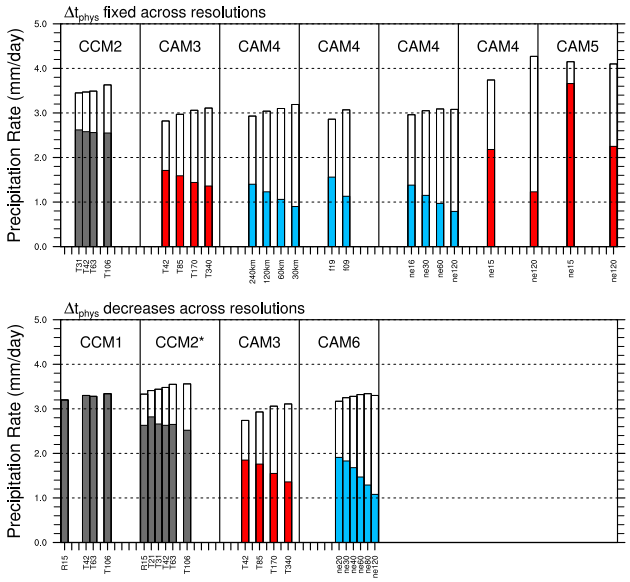


**Figure 1.** Bar-graph of the convective (solid) and grid-scale (white) climatological precipitation rates in prior CAM/CCM convergence studies. Each window contains a single convergence study, with identical x-axis; the approximate grid resolution. Colors indicate the model configuration; January ensemble (black) and aqua-planet configurations with SST profiles $QOBS$ (blue) and $CNTL$ (red) after Neale and Hoskins (2000). Studies included in this figure are Kiehl and Williamson (1991) (CCM1), Williamson *et al.* (1995) (CCM2), Williamson (2008) (CAM3), Rauscher *et al.* (2013); Zarzycki *et al.* (2014); Herrington and Reed (2017) (CAM4), Zarzycki *et al.* (2014) (CAM5) and this study (CAM6). CCM2* refers to the modified parameter experiment of Williamson *et al.* (1995), where parameters vary with resolution to reduce the dependence of cloud fraction on resolution.

argue that the $-\frac{5}{3}$ slope being common in both observations and models provides an emergent constraint for $b = \frac{1}{3}$ and $n = -\frac{2}{3}$.

In large-eddy simulations, the sensitivity of vertical velocities to resolution is adequately explained by a scale analysis of the dynamical equations (Weisman *et al.* 1997; Pauluis and Garner 2006; Jeevanjee and Romps 2016). For hydrostatic scales relevant to AGCMs, a scale analysis of the Poisson equation gives $W \propto D^{-1}$, where $D$ is the horizontal scale of a buoyancy perturbation driving vertical motion (Herrington and Reed 2018). In CAM aqua-planet simulations, the largest source of buoyancy is from grid-scale cloud formation, whose horizontal extents are set by the effective resolution of the model (i.e., some multiple of $\Delta x$), indicating $n = -1$ (Herrington and Reed 2018). Herrington and Reed (2017) has shown that the $n = -1$ scaling does not explain the behavior of CAM4 in a convergence experiment, but follow-up studies (Herrington and Reed 2018; Herrington *et al.* 2019) indicate that the inadequacy of the $n = -1$ scaling is not definitive due to time-truncation errors associated with fixing the physics time-step ($\Delta t_{phys}$) across resolutions in that study.

Another robust response of the CAM/CCM lineage to resolution is an increase in stratiform precipitation rates (i.e., the precipitation from grid-scale clouds), at the expense of parameterized convective precipitation rates. This behavior is summarized in Figure 1, which is a bar-graph of the climatological, global mean stratiform and convective precipitation rates in prior CAM/CCM convergence studies. The propensity for precipitation rates to shift from the convective to the stratiform scheme with resolution has been documented in other AGCMs as well (Pope and Stratton 2002; Terai *et al.* 2018), but none have given a satisfactory explanation for this sensitivity. The studies of Kiehl and Williamson (1991), Williamson *et al.* (1995) and Williamson (2013) indicate that the tendency to reduce $\Delta t_{phys}$ with resolution would by itself reduce the convective precipitation rates, however Figure 1 (top row) indicates that convergence studies with fixed $\Delta t_{phys}$ still show a reduction in convective precipitation rates with resolution.

In this study, a convergence experiment using CAM, version 6 (CAM6; https://ncar.github.io/CAM/doc/build/html/users_guide/index.html) is carried out and analyzed in detail. It is shown that the resolution sensitivity of vertical velocities are well described with $n = -1$ in equation (1), provided $\Delta t_{phys}$ is defined in a way that avoids large truncation errors across resolutions. The reduction in convective precipitation rates with resolution in CAM6 is shown to result from the greater magnitude subsiding motion, creating a more stable atmosphere in which the criterion for parameterized convection occurs less often. The feedback of the resolved vertical motion on the physics indicates that the root cause of resolution sensitivity in CAM arises from the sensitivity of resolved dynamical modes to native grid resolution. Section 2 describes CAM6 and details the convergence experiment. Section 3 contains a thorough analysis of the CAM6 simulations and Section 4 provides some discussion and conclusions.

## 2. Methods

### 2.1. *Dynamical Core*

This study uses the spectral-element dynamical core option of Community Atmosphere Model (CAM-SE; Dennis *et al.* 2012), coupled with a mass conserving, semi-Lagrangian advection method for accelerated multi-tracer transport (CSLAM; Lauritzen *et al.* 2017), and dry-mass vertical coordinate with comprehensive treatment of moisture and energy (Lauritzen *et al.* 2018). The dry dynamics are solved using the high-order, momentum, mass and energy conserving spectral element method (Taylor and Fournier 2010), with the elements defined by a cubed-sphere grid. The notation for the horizontal grid resolution is an '$ne$' followed by the number of elements making up an edge of one cubed-sphere face, e.g., $ne30$. Hyper-viscous $\nabla^4$ explicit numerical dissipation is applied to temperature, dry pressure thickness, rotational and divergent winds. CSLAM tracer transport uses a finite volume grid constructed from the cubed-sphere of elements, and contains the same degrees of freedom as the dry dynamics.

### 2.2. *Physical Parameterizations*

The physics are evaluated on the finite-volume CSLAM grid, and the tendencies mapped back to the spectral element grid. The coupled system, referred to as CAM-SE-CSLAM, conserves energy, mass and preserves linear correlations between two reactive species to within machine precision (Herrington *et al.* 2018). A coarser physics grid, containing $\frac{5}{9}$ fewer degrees of freedom than the dynamical core grid is also available as part of the CAM-SE-CSLAM package (Herrington *et al.* 2019). This lower-resolution physics grid is used in this study, but only as a member of a perturbed parameter ensemble and not in the default convergence experiment. The dynamics time-step is subcycled within a longer physics time-step $\Delta t_{phys}$, and the temperature and momentum increments from the physics are divided by the number of subcycles and added to the dynamical core at the beginning of each subcycle. The full moisture increment from the physics is applied only at the start of the first subcycle to conserve tracer mass ($ftype = 2$ option in Lauritzen *et al.* 2018).

The simulations use the CAM6 physics package. The Cloud Layers Unified by Binormals (CLUBB Golaz *et al.* 2002; Bogenschutz *et al.* 2013) is an assumed probability distribution function (PDF) high-order closure model that handles shallow convection, planetary boundary layer mixing and cloud macrophysics. The macrophyiscs are coupled with a two-moment bulk cloud microphysics scheme with prognostic precipitation (Gettelman *et al.* 2015), and microphysics are coupled with a three mode Modular Aerosol Model (Liu *et al.* 2012). The

combined macrophysics/microphysics routines generate grid-scale clouds with stratiform precipitation. Deep convection is parameterized using a quasi-equilibrium mass flux scheme (Zhang and McFarlane 1995) and a dilute form of the convective available potential energy (CAPE) is computed and used as the convective trigger (convection occurs if dilute CAPE $\geq 70$ J/kg), and for closing the mass fluxes in the cloud ensemble (Neale *et al.* 2008). The deep convection scheme also parameterizes convective momentum transport (Richter and Rasch 2008).

### 2.3. *Experimental Design*

The convergence experiment is performed in an aqua-planet configuration (Neale and Hoskins 2000; Medeiros *et al.* 2016), an all ocean planet with fixed, zonally symmetric sea surface temperatures modeled after present day Earth ($QOBS$ in Neale and Hoskins 2000). The aqua-planets are in a perpetual equinox, and aerosols are largely absent from the simulations. Each simulation is ran for one simulated year. Six different horizontal grids are used in this study, which are provided in Table 1. All analyses exclude the first month of the simulations, and are computed on their native grids unless otherwise stated.

The horizontal hyper-viscosity operators $\nu$ vary with resolution after Herrington *et al.* (2019), also provided in Table 1. The values of $\nu$ are a factor 2.5 greater for divergence damping and are not shown. $\Delta t_{phys}$ is chosen to scale with resolution, in proportion to the grid spacing,

$$\Delta t_{phys} = \Delta t_{phys,0} \times \frac{n_{e,0}}{n_e}\ s, \tag{2}$$

where $\Delta t_{phys,0}$ is taken to be the standard 1800 s used in CAM-SE-CSLAM at the standard resolution, $n_{e,0} = ne30$ (equivalent to an average equatorial grid spacing $\Delta x = 111.2$km). This scaling was chosen to avoid large time-truncation errors in a rising moist bubble test (Appendix A in Herrington *et al.* 2019), and it is understood that this choice of $\Delta t_{phys}$ will likely lead to greater resolution sensitivity (Williamson 2008). The convective time-scale in the deep convection scheme is fixed at 3600 s in all simulations.

## 3. Results

Table 1 provides globally averaged, climatological metrics for the CAM6 simulations which are typically published in CAM/CCM convergence studies. Total precipitable water, total cloud fraction and deep convective precipitation rate decreases, while stratiform precipitation increases, monotonically with resolution. Resolution sensitivity in CAM6 is similar to all prior versions of the model.

### 3.1. *Vertical Velocities and Resolution*

The PDF of negative, or upward vertical pressure velocities $\omega$ in the aqua-planets is shown in Figure 2a. The magnitude of upward $\omega$ increases monotonicaly with resolution, with positive, or downward $\omega$ behaving similarly (not shown). This monotonic increase in the magnitude of $\omega$ is evident even after remapping all the model output to a common grid ($ne20$; dotted curves Figure 2a).

The PDF's may be scaled to the highest-resolution resolution grid through $P(\omega)_s = \alpha P(\omega/\alpha)$, where $\alpha$ is the scale factor from equation 1, and setting $\Delta x_0$ to the $ne120$ grid-spacing. Figure 2b shows the scaled PDFs using $n = -1$ in equation 1. The scaled PDF's all collapse onto the high-resolution reference, indicating that the power-law with $n = -1$ explains to first-order the variation in vertical velocity with resolution in the aqua-planet simulations.

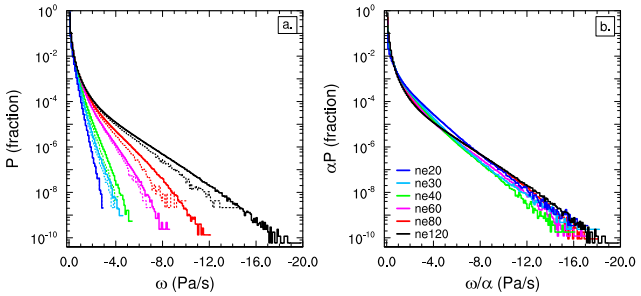


**Figure 2.** Probability density distribution of the upward vertical pressure velocities $\omega$ computed everywhere in the model from six-hourly output over the entirety of the year-long simulations. (a) Values on their native grid (solid) and values remapped to the $ne20$ grid (dotted), (b) values on their native grid, scaled to the $ne120$ resolution.

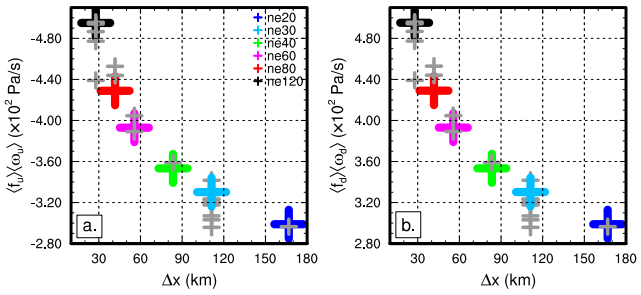


**Figure 3.** (a,b,c,e,f,g) Components of the global mean vertical pressure velocity, (a) $\overline{\langle f_u \rangle \langle \omega_u \rangle}$ (b) $\overline{\langle f_d \rangle \langle \omega_d \rangle}$. Colors are as in Figure 2. Grey crosses are for the perturbed parameter runs.

Changes to the vertical velocity field can be further understood through decomposing the mass weighted vertical mean $\omega$ into upward and downward components,

$$\langle \omega \rangle = \langle f_u \rangle \langle \omega_u \rangle + \langle f_d \rangle \langle \omega_d \rangle, \tag{3}$$

where $\langle f_x \rangle$ and $\langle \omega_x \rangle$ refers to the vertical mass fraction $\left(\frac{\int dp_x}{\int dp}\right)$ and the $x$ component of the mass weighted vertical mean of $\omega$ $\left(\frac{\int \omega_x dp_x}{\int dp_x}\right)$, respectively, subscript $u$ refers to upward motion and $d$, downward motion.

The global mean, climatological components $\langle f_u \rangle \langle \omega_u \rangle$ and $\langle f_d \rangle \langle \omega_d \rangle$ are provided in Figure 3a,b for the aqua-planet simulations. The magnitude of both $\langle f_u \rangle \langle \omega_u \rangle$ and $\langle f_d \rangle \langle \omega_d \rangle$ increase monotonically with resolution, and are equal and opposite, which is a requirement of mass conservation in the model and a convenient check of the calculation. While $\langle f_d \rangle$ is about 25% larger than $\langle f_u \rangle$ in all simulations, the vertical mass fractions varies by only few percent with resolution, and so the monotonic behavior of $\langle f_x \rangle \langle \omega_x \rangle$ with resolution is primarily from variations in $\langle \omega_x \rangle$ (not shown).

### 3.2. *Vertical Velocities and Convective Precipitation*

The Zhang and McFarlane (1995) deep convection scheme (referred to as the $ZM$ scheme, hereafter) is modulated by the dilute CAPE calculation, which itself is intertwined with the vertical velocity field (Song and Zhang 2018). The CAPE budget can be separated into two components (Zhang 2002); instability due to the thermodynamic state of parcels in the boundary layer and the instability generated through advection of dry static energy and moisture by the environment, i.e., the resolved flow. The latter term is defined as,

$$-R_d \int_{p_t}^{p_b} \frac{\partial T_{ve}}{\partial t} d\ln p \tag{4}$$

Table 1. Experimental design and global mean climatologies.

| Variable | $ne20$ | $ne30$ | $ne40$ | $ne60$ | $ne80$ | $ne120$ |
|---|---|---|---|---|---|---|
| $\Delta x$ (km) | 166.8 | 111.2 | 83.4 | 55.6 | 41.7 | 27.8 |
| $\nu\ (m^4/s)$ | $1.5 \times 10^{15}$ | $4.0 \times 10^{14}$ | $1.5 \times 10^{14}$ | $4.0 \times 10^{13}$ | $1.5 \times 10^{13}$ | $4.0 \times 10^{12}$ |
| $\Delta t_{phys}$ (s) | 2700 | 1800 | 1350 | 900 | 675 | 450 |
| Total Cloud Fraction | 0.844 | 0.835 | 0.824 | 0.810 | 0.804 | 0.800 |
| Total Precipitable Water (mm) | 23.31 | 23.01 | 22.62 | 22.25 | 21.93 | 21.72 |
| Convective Precipitation (mm/day) | 1.91 | 1.83 | 1.68 | 1.47 | 1.29 | 1.08 |
| Stratiform Precipitation (mm/day) | 1.26 | 1.42 | 1.60 | 1.85 | 2.05 | 2.22 |

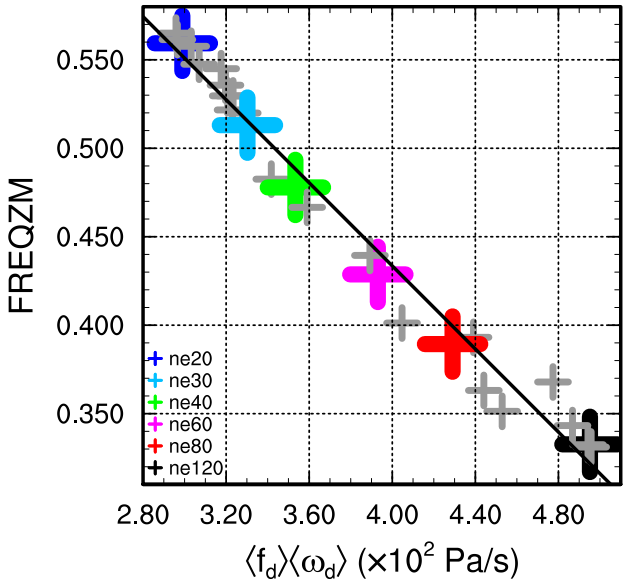


**Figure 4.** Scatter plot of $\overline{\langle f_d \rangle}\ \overline{\langle \omega_d \rangle}$ and FREQZM, and the fitted linear regression which has a Pearson's R-value = 0.99. Colors are as in Figure 2. Grey crosses are for the perturbed parameter ensemble.

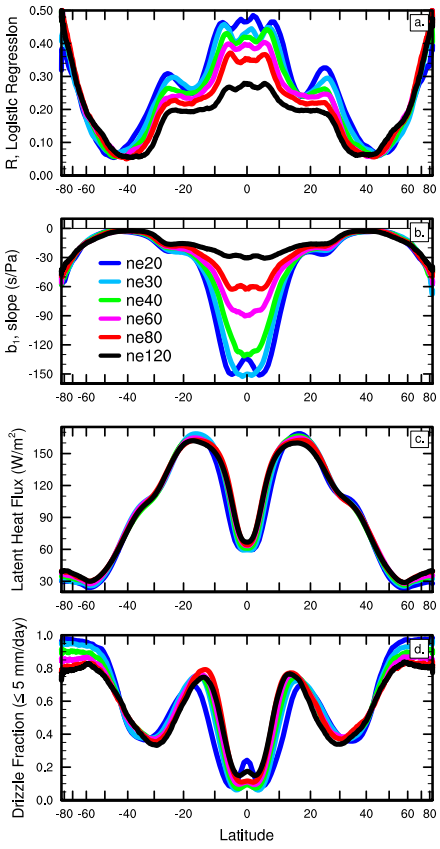


**Figure 5.** Zonal mean (a) R-values and (b) sensitivity parameter in the logistic regression, (d) time mean surface latent heat fluxes and (c) drizzle fraction. Colors are as in Figure 2.

where $T_{ve}$ is the virtual temperature of the environment, $R_d$ the gas constant for dry air and subscripts $b$ and $t$ refer to the parcel launch level (typically in the boundary layer) and the level of neutral buoyancy, respectively (Zhang 2002). Equation 4 shows that warming the environment reduces CAPE though reducing the buoyancy of lifted air parcels. The $T_{ve}$ budget contains a term; the vertical advection of potential energy, which simplifies to $\frac{w}{c_{pd}}\frac{\partial gz}{\partial z} = \frac{g}{c_{pd}}w$, and directly proportional to the vertical velocity $w$ by the factor $\frac{g}{c_{pd}}$, with $g$ the acceleration of gravity and $c_{pd}$ the specific heat capacity of dry air (F. Song, personal communication). In subsiding regions, $w$ is negative and opposes the generation of CAPE through adiabatic warming of the environment.

There is an excellent negative correlation (Pearson's R-value = 0.99) between the global mean, climatological $\langle f_d \rangle \langle \omega_d \rangle$ and a measure of the activity of the ZM scheme in the simulations, global mean, climatological $FREQZM$ (Figure 4). At any given grid-point and time-step, $FREQZM$ is a binary variable: one if the ZM scheme is active, zero if it is not. Time-mean $FREQZM$ therefore indicates the fraction of the model time that the ZM scheme is triggered, i.e., dilute CAPE exceeds $\geq 70$ J/kg. It is hypothesized that the greater subsiding motion with resolution opposes the generation of dilute CAPE through subsidence warming, reducing the frequency the ZM scheme is triggered, and creating the strong negative correlation in Figure 4.

### 3.3. *Convection Activity and Atmospheric Stability*

To test the hypothesis, a logistic regression between subsiding motion and $FREQZM$ is performed for each grid column within each of the simulations. Logistic regression uses an iterative method to fit a continuous variable predictor, $x$ to a binary predictand $p$ through the exponential (Wilks 2011),

$$p = \frac{exp[b_0 + b_1 x]}{1 + exp[b_0 + b_1 x]}, \tag{5}$$

where $b_0$ and $b_1$ are the shape parameters of the exponential. The predictor is then the instantaneous $\langle f_d \rangle \langle \omega_d \rangle$ of a grid column, and the predictand the binary $FREQZM$. Since the aqua-planets have zonally symmetric boundary conditions, there is a zonally varying structure in the goodness of fit (R-value) and parameter $b_1$ (hereafter referred to as the sensitivity parameter; Figure 5a,b).

The zonal mean R-values indicates the greatest goodness of fit in the deep tropics ($\pm 10^\circ$ latitude). Figure 5c shows the climatological, zonal-mean latent heat flux in the simulations, which is expected to contribute positively to CAPE through the component associated with the thermodynamic state of boundary layer parcels. In the deep tropics, the latent heat flux is small, and the sensitivity parameter is large and negative (Figure 5b), which is consistent with our hypothesis that the subsiding motion actively depresses CAPE and the activity of the ZM scheme in the simulations. The sensitivity parameter becomes less negative in the deep tropics with resolution, likely due to the greater magnitude $\langle f_d \rangle \langle \omega_d \rangle$ with resolution, which requires a lower sensitivity parameter to predict the binary of whether the ZM

Table 2. Fractional contribution of latitude bands $\pm 10^\circ$ and $\pm 15^\circ$ to changes in global mean precipitation with resolution. The grid headers refer to differences with respect to the next lowest grid resolution, e.g., $ne30 = ne30 - ne20$, $ne40 = ne40 - ne30$, etc..., which are computed through remapping all data to the $ne20$ grid.

| Variable | $ne30$ | $ne40$ | $ne60$ | $ne80$ | $ne120$ |
|---|---|---|---|---|---|
| $\pm 10^\circ$ (17.6% of global area) | | | | | |
| Convective Precipitation | -0.58 | 0.62 | 0.66 | 0.72 | 0.70 |
| Stratiform Precipitation | 0.55 | 0.63 | 0.69 | 0.67 | 0.41 |
| $\pm 15^\circ$ (25.8% of global area) | | | | | |
| Convective Precipitation | 0.22 | 0.75 | 0.73 | 0.79 | 0.72 |
| Stratiform Precipitation | 0.46 | 0.64 | 0.71 | 0.70 | 0.49 |

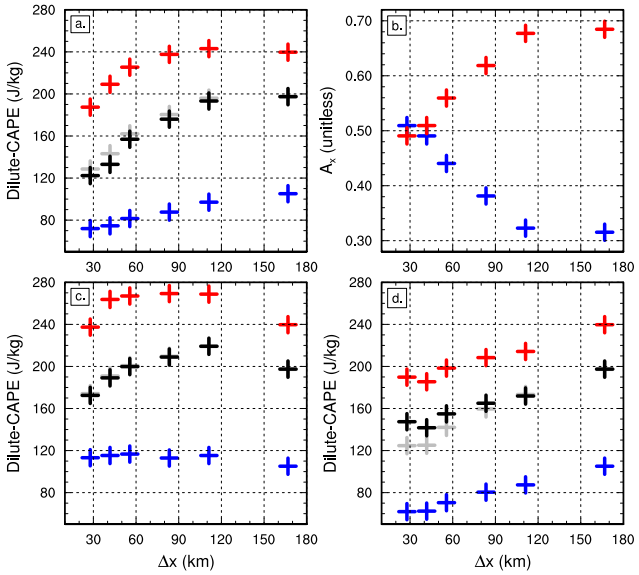


**Figure 6.** (a) time mean fraction of the deep tropics in the simulations with upward $\langle\omega\rangle$ (red) and downward $\langle\omega\rangle$ (blue), (b) CAPE computed from the mean temperature and moisture profiles of upward regions and downward regions. Black is for CAPE computed from the mean temperature and moisture profiles for the entire deep tropics, grey is the approximate discussed in the text.

scheme is active. The R-values generally decrease with resolution indicating that there is degradation in the relationship with resolution. All values shown are statistically significant at the 95% level using a log-likelihood test (Wilks 2011).

To understand the degree to which atmospheric stability in the deep tropics is dependent on ascending and descending motion, temperature and moisture profiles are conditionally sampled based on whether $\langle\omega\rangle$ is positive or negative, indicating predominantly subsiding or ascending grid columns. The mean temperature and moisture profiles of subsiding and ascending regions in the deep tropics are used to compute the dilute-CAPE used by the ZM scheme, offline. Figure 6a indicates that the mean profile of ascending regions are associated with large values of CAPE ($> 180$ J/kg), and low values in subsiding regions ($< 110$ J/kg). Figure 8 shows the climatological temperature and specific humidity profiles of subsiding grid cells, averaged over the deep tropics and presented as anomalies from the mean temperature and specific humidity of the entire deep Tropics. The mean profiles of subsiding regions have an anomalous warming layer in the $600 - 800$ hPa layer and an anomalous moisture deficit throughout the entire column. This warming of the environment in subsiding regions opposes the generation of CAPE through equation 4.

Figure 6b shows that fractional area of air columns in the deep tropics that are predominantly subsiding (ascending) changes drastically with resolution, from 0.32 (0.68) in the $ne20$ ($\Delta x = 166.8$ km) run, and monotonically increasing (decreasing) with resolution to 0.51 (0.49) in the $ne120$ ($\Delta x = 27.8$ km) run. Interestingly, the sum of the product of the fractional areas with their corresponding CAPE values gives approximately the

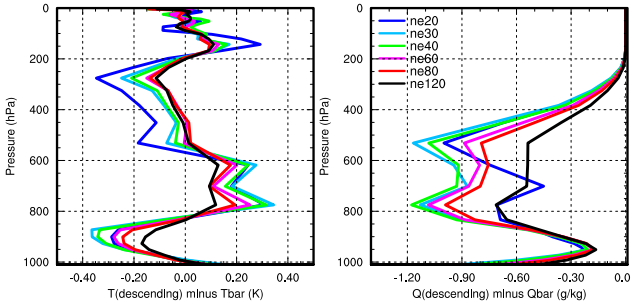


**Figure 7**

same CAPE values computed from the mean temperature and moisture profiles over the entire deep tropics (Figure 6a). This provides strong evidence that CAPE values in the deep tropics are decreasing with resolution because a larger (smaller) space-time fraction of the deep tropics are made up of predominantly subsiding (ascending) grid columns with increasing resolution.

### 3.4. *Vertical Velocities and Stratiform Precipitation*

### 3.5. *Biases Unrelated to Resolution*

Poleward of the deep tropics and within the subtropics, the logistic regression indicates that subsidence is a poor predictor of $FREQZM$ (Figure 5a,b). The R-value decreases to a local minimum between $15^\circ - 20^\circ$ latitude, and the magnitude of the sensitivity parameter steeply declines. The local minimum in the R-value corresponds with a local maximum in the latent heat fluxes (Figure 5c), indicating that the boundary layer is being driven unstable by large surface latent heat fluxes. The CAPE values in the $10^\circ - 15^\circ$ latitude region are likely to be small, since the ZM precipitation rate consists primarily of drizzle (Figure 5d). The predominance of drizzle in this region is probably a result of the large subsiding motion in the subtropics (not shown) constraining CAPE from becoming too large. AGCMs are known to suffer from an excess drizzle bias in precisely this region (Dai 2006), and this analysis indicates that this bias is due to the use of a CAPE trigger function.

## Acknowledgement

This class file was developed by Sunrise Setting Ltd, Paignton, Devon, UK. Website:
www.sunrise-setting.co.uk

## References

Arakawa A, Wu CM. 2013. A unified representation of deep moist convection in numerical modeling of the atmosphere. part i. *Journal of the Atmospheric Sciences* **70**(7): 1977–1992.

Bogenschutz PA, Gettelman A, Morrison H, Larson VE, Craig C, Schanen DP. 2013. Higher-order turbulence closure and its impact on climate simulations in the community atmosphere model. *Journal of Climate* **26**(23): 9655–9676.

Cho JY, Zhu Y, Newell RE, Anderson BE, Barrick JD, Gregory GL, Sachse GW, Carroll MA, Albercook GM. 1999. Horizontal wavenumber spectra of winds, temperature, and trace gases during the pacific exploratory missions: 1. climatology. *Journal of Geophysical Research: Atmospheres* **104**(D5): 5697–5716.

Dai A. 2006. Precipitation characteristics in eighteen coupled climate models. *Journal of Climate* **19**(18): 4605–4630.

Dennis JM, Edwards J, Evans KJ, Guba O, Lauritzen PH, Mirin AA, St-Cyr A, Taylor MA, Worley PH. 2012. CAM-SE: A scalable spectral element dynamical core for the Community Atmosphere Model. *Int. J. High. Perform. C.* **26**(1): 74–89, doi:10.1177/1094342011428142, URL http://hpc.sagepub.com/content/26/1/74.abstract.

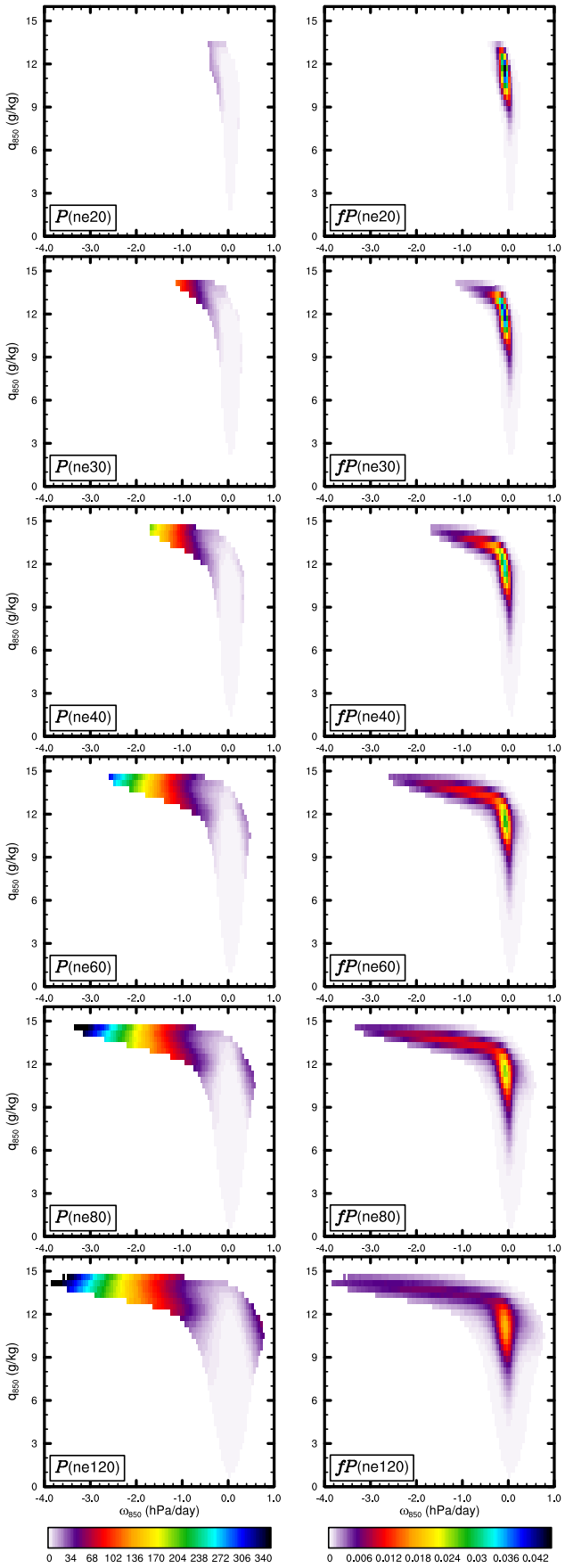


**Figure 8**

Donner LJ, O'Brien TA, Rieger D, Vogel B, Cooke WF. 2016. Are atmospheric updrafts a key to unlocking climate forcing and sensitivity? *Atmospheric Chemistry and Physics* **16**(20): 12 983–12 992.

Germano M. 1992. Turbulence: the filtering approach. *Journal of Fluid Mechanics* **238**: 325–336.

Gettelman A, Morrison H, Santos S, Bogenschutz P, Caldwell P. 2015. Advanced two-moment bulk microphysics for global models. part ii: Global model solutions and aerosol–cloud interactions. *Journal of Climate* **28**(3): 1288–1307.

Golaz JC, Larson VE, Cotton WR. 2002. A pdf-based model for boundary layer clouds. part i: Method and model description. *Journal of the Atmospheric Sciences* **59**(24): 3540–3551, doi:10.1175/1520-0469(2002)059⟨3540:apbmfb⟩2.0.co;2.

Harris LM, Lin SJ, Tu C. 2016. High-resolution climate simulations using gfdl hiram with a stretched global grid. *Journal of Climate* **29**(11): 4293–4314, doi:10.1175/jcli-d-15-0389.1.

Herrington A, Lauritzen P, Taylor MA, Goldhaber S, Eaton BE, Bacmeister J, Reed K, Ullrich P. 2018. Physics-dynamics coupling with element-based high-order galerkin methods: quasi equal-area physics grid. *Mon. Wea. Rev.* **47**: 69–84, doi:10.1175/MWR-D-18-0136.1.

Herrington A, Reed K. 2018. An idealized test of the response of the community atmosphere model to near-grid-scale forcing across hydrostatic resolutions. *J. Adv. Model. Earth Syst.* **10**(2): 560–575.

Herrington AR, Lauritzen PH, Reed KA, Goldhaber S, Eaton BE. 2019. Exploring a lower resolution physics grid in cam-se-cslam. *Journal of Advances in Modeling Earth Systems* **11**.

Herrington AR, Reed KA. 2017. An explanation for the sensitivity of the mean state of the community atmosphere model to horizontal resolution on aquaplanets. *J. Climate* **30**(13): 4781–4797, doi:10.1175/jcli-d-16-0069.1, URL http://dx.doi.org/10.1175/jcli-d-16-0069.1.

Jeevanjee N. 2017. Vertical velocity in the gray zone. *Journal of Advances in Modeling Earth Systems* **9**(6): 2304–2316, doi:10.1002/2017MS001059.

Jeevanjee N, Romps DM. 2016. Effective buoyancy at the surface and aloft. *Quart. J. Roy. Meteor. Soc.* **142**(695): 811–820.

Kiehl J, Williamson D. 1991. Dependence of cloud amount on horizontal resolution in the national center for atmospheric research community climate model. *Journal of Geophysical Research: Atmospheres* **96**(D6): 10 955–10 980.

Lauritzen PH, Nair R, Herrington A, Callaghan P, Goldhaber S, Dennis J, Bacmeister JT, Eaton B, Zarzycki C, Taylor MA, Gettelman A, Neale R, Dobbins B, Reed K, Dubos T. 2018. NCAR CESM2.0 release of CAM-SE: A reformulation of the spectral-element dynamical core in dry-mass vertical coordinates with comprehensive treatment of condensates and energy. *J. Adv. Model. Earth Syst.* doi:10.1029/2017MS001257.

Lauritzen PH, Taylor MA, Overfelt J, Ullrich PA, Nair RD, Goldhaber S, Kelly R. 2017. CAM-SE-CSLAM: Consistent coupling of a conservative semi-lagrangian finite-volume method with spectral element dynamics. *Mon. Wea. Rev.* **145**(3): 833–855, doi:10.1175/MWR-D-16-0258.1.

Liu X, Easter RC, Ghan SJ, Zaveri R, Rasch P, Shi X, Lamarque JF, Gettelman A, Morrison H, Vitt F, *et al.* 2012. Toward a minimal representation of aerosols in climate models: Description and evaluation in the community atmosphere model cam5. *Geoscientific Model Development* **5**(3): 709.

Medeiros B, Williamson DL, Olson JG. 2016. Reference aquaplanet climate in the community atmosphere model, version 5. *J. Adv. Model. Earth Syst.* **8**(1): 406–424, doi:10.1002/2015MS000593.

Nastrom GD, Gage KS. 1985. A climatology of atmospheric wavenumber spectra of wind and temperature observed by commercial aircraft. *J. Atmos. Sci.* **42**: 950–960.

Neale RB, Chen CC, Gettelman A, Lauritzen PH, Park S, Williamson DL, Conley AJ, Garcia R, Kinnison D, Lamarque JF, Marsh D, Mills M, Smith AK, Tilmes S, Vitt F, Cameron-Smith P, Collins WD, Iacono MJ, Easter RC, Ghan SJ, Liu X, Rasch PJ, Taylor MA. 2012. Description of the NCAR Community Atmosphere Model (CAM 5.0). NCAR Technical Note NCAR/TN-486+STR, National Center of Atmospheric Research.

Neale RB, Chen CC, Gettelman A, Lauritzen PH, Park S, Williamson DL, Conley AJ, Garcia R, Kinnison D, Lamarque JF, Marsh D, Mills M, Smith AK, Tilmes S, Vitt F, Cameron-Smith P, Collins WD, Iacono MJ, Easter RC, Ghan SJ, Liu X, Rasch PJ, Taylor MA. 2010. Description of the NCAR Community Atmosphere Model (CAM 4.0). NCAR Technical Note, National Center of Atmospheric Research.

Neale RB, Hoskins BJ. 2000. A standard test for agcms including their physical parametrizations: I: the proposal. *Atmos. Sci. Lett* **1**(2): 101–107, doi:10.1006/asle.2000.0022.

Neale RB, Richter JH, Jochum M. 2008. The impact of convection on ENSO: From a delayed oscillator to a series of events. *J. Climate* **21**: 5904–5924.

O'Brien TA, Collins WD, Kashinath K, Rübel O, Byna S, Gu J, Krishnan H, Ullrich PA. 2016. Resolution dependence of precipitation statistical fidelity in hindcast simulations. *J. Adv. Model. Earth Syst.* **8**(2): 976–990, doi:10.1002/2016ms000671, URL http://dx.doi.org/10.1002/2016ms000671.

Orlanski I. 1981. The quasi-hydrostatic approximation. *J. Atmos. Sci.* **38**: 572–582, doi:10.1175/1520-0469(1981)038⟨0572:TQHA⟩2.0.CO;2, URL http://dx.doi.org/10.1175/1520-0469(1981)038<0572:TQHA>2.0.CO;2.

Pauluis O, Garner S. 2006. Sensitivity of radiative–convective equilibrium simulations to horizontal resolution. *J. Atmos. Sci.* **63**(7): 1910–1923.

Plant RS, Craig GC. 2008. A stochastic parameterization for deep convection based on equilibrium statistics. *J. Atmos. Sci.* **65**: 87–105, doi:10.1175/2007JAS2263.1, URL http://dx.doi.org/10.1175/2007JAS2263.1.

Pope V, Stratton R. 2002. The processes governing horizontal resolution sensitivity in a climate model. *Climate Dynamics* **19**(3-4): 211–236.

Rauscher SA, O'Brien TA, Piani C, Coppola E, Giorgi F, Collins WD, Lawston PM. 2016. A multimodel intercomparison of resolution effects on precipitation: simulations and theory. *Climate Dynamics* **47**(7-8): 2205–2218, doi:10.1007/s00382-015-2959-5.

Rauscher SA, Ringler TD, Skamarock WC, Mirin AA. 2013. Exploring a global multiresolution modeling approach using aquaplanet simulations. *Journal of Climate* **26**(8): 2432–2452, doi:10.1175/jcli-d-12-00154.1.

Richter JH, Rasch PJ. 2008. Effects of convective momentum transport on the atmospheric circulation in the community atmosphere model, version 3. *J. Climate* **21**(7): 1487–1499.

Skamarock WC, Klemp JB, Duda MG, Fowler L, Park SH, Ringler TD. 2012. A multi-scale nonhydrostatic atmospheric model using centroidal Voronoi tesselations and C-grid staggering. *Mon. Wea. Rev.* **240**: 3090–3105, doi: doi:10.1175/MWR-D-11-00215.1.

Song F, Zhang GJ. 2018. Understanding and improving the scale dependence of trigger functions for convective parameterization using cloud-resolving model data. *Journal of Climate* **31**(18): 7385–7399.

Taylor MA, Fournier A. 2010. A compatible and conservative spectral element method on unstructured grids. *J. Comput. Phys.* **229**(17): 5879 – 5895, doi: 10.1016/j.jcp.2010.04.008.

Terai CR, Caldwell PM, Klein SA, Tang Q, Branstetter ML. 2018. The atmospheric hydrologic cycle in the acme v0. 3 model. *Climate dynamics* **50**(9-10): 3251–3279.

Ullrich PA, Jablonowski C, Kent J, Lauritzen PH, Nair R, Reed KA, Zarzycki CM, Hall DM, Dazlich D, Heikes R, Konor C, Randall D, Dubos T, Meurdesoif Y, Chen X, Harris L, Kühnlein C, Lee V, Qaddouri A, Girard C, Giorgetta M, Reinert D, Klemp J, Park SH, Skamarock W, Miura H, Ohno T, Yoshida R, Walko R, Reinecke A, Viner K. 2017. "dcmip2016: A review of non-hydrostatic dynamical core design and intercomparison of participating models". *Geosci. Model Dev.* **10**: 4477–4509, doi:10.5194/gmd-10-4477-2017.

Weisman ML, Skamarock WC, Klemp JB. 1997. The resolution dependence of explicitly modeled convective systems. *Monthly Weather Review* **125**(4): 527–548, doi:10.1175/1520-0493(1997)125⟨0527:TRDOEM⟩2.0.CO;2.

Wilks DS. 2011. *Statistical methods in the atmospheric sciences*, vol. 100. Academic press.

Williamson DL. 2008. Convergence of aqua-planet simulations with increasing resolution in the community atmospheric model, version 3. *Tellus A* **60**(5): 848–862, doi:10.1111/j.1600-0870.2008.00339.x.

Williamson DL. 2013. The effect of time steps and time-scales on parametrization suites. *Quart. J. Roy. Meteor. Soc.* **139**(671): 548–560, doi: 10.1002/qj.1992.

Williamson DL, Kiehl JT, Hack JJ. 1995. Climate sensitivity of the ncar community climate model (ccm2) to horizontal resolution. *Climate Dynamics* **11**(7): 377–397, doi:10.1007/s003820050082.

Yang Q, Leung LR, Rauscher SA, Ringler TD, Taylor MA. 2014. Atmospheric moisture budget and spatial resolution dependence of precipitation extremes in aquaplanet simulations. *Journal of Climate* **27**(10): 3565–3581, doi:10.1175/jcli-d-13-00468.1.

Zarzycki CM, Levy MN, Jablonowski C, Overfelt JR, Taylor MA, Ullrich PA. 2014. Aquaplanet experiments using cam's variable-resolution dynamical core. *J. Climate* **27**(14): 5481–5503, doi:10.1175/JCLI-D-14-00004.1.

Zhang G, McFarlane N. 1995. Sensitivity of climate simulations to the parameterization of cumulus convection in the canadian climate centre general circulation model. *Atmosphere-ocean* **33**(3): 407–446.

Zhang GJ. 2002. Convective quasi-equilibrium in midlatitude continental environment and its effect on convective parameterization. *Journal of Geophysical Research: Atmospheres* **107**(D14): ACL–12.

Zängl G, Reinert D, Rípodas P, Baldauf M. 2014. The icon (icosahedral non-hydrostatic) modelling framework of dwd and mpi-m: Description of the non-hydrostatic dynamical core. *Quarterly Journal of the Royal Meteorological Society* **141**(687): 563–579, doi:10.1002/qj.2378.

 